Influence of Obliquely Propagating Monsoon Gravity Waves on Southern Polar Summer Mesosphere after Stratospheric Sudden Warmings in Winter Stratosphere

Enter authors here: D. Alexandre[1,3], B. Thurairajah[2,3], S. L. England[1,3], and C. Y. Cullens[4]

[1]Aerospace and Ocean Engineering department.

[2]Electrical and Computer Engineering department.

[3]Virginia Polytechnic Institute and State University, Blacksburg VA, USA.

[4]University of California Berkeley, Berkeley CA, USA.

Corresponding author: David Alexandre (davida49@vt.edu)

Key Points:

- Polar mesospheric clouds in the SH correlate with gravity waves from monsoon regions indicating oblique propagation of gravity waves in SH
- Gravity wave propagation in high-latitude winter hemisphere is at mid latitudes and slanted equatorward during stratospheric sudden warmings
- Stratospheric sudden warmings appear to change the oblique propagation path of monsoon generated gravity waves in summer hemisphere

Abstract

Oblique propagation of gravity waves (GWs) refers to latitudinal propagation (or vertical propagation away from their source) from the low latitude troposphere to the polar mesosphere. This propagation is not included in current gravity wave parameterization schemes, but may be an important component of the global dynamical structure. Previous studies have revealed a high correlation between observations of GW Momentum Flux (GWMF) from monsoon convection and Polar Mesospheric Clouds (PMCs) in the northern hemisphere. In this work, we report on data and model analysis of the effects of Stratospheric Sudden Warmings (SSWs) in the northern hemisphere, on the oblique propagation of GWs from the southern hemisphere tropics, that in turn influence PMCs in the southern summer mesosphere. In response to SSWs, vertical propagation of GWs from high-latitude winter hemisphere is at mid latitudes and appears more slanted toward the equator with increasing altitude, following the weaker stratospheric eastward jet. The oblique propagation of GWs from southern monsoon regions tends to start at higher altitudes with a sharper poleward slanted structure towards the summer mesosphere. The correlation between PMCs in summer southern hemisphere and the zonal GWMF from 50°N to 50°S exhibits a high-correlation pattern that connects the winter stratosphere with the summer mesosphere, indicating the influence of inter-hemispheric coupling mechanism. Temperature and wind anomalies suggest that the dynamics in winter hemisphere can influence the equatorial region, which in turn, can influence the oblique propagation of monsoon GWs.

Plain Language Summary

Propagation of waves throughout Earth atmosphere is a key phenomenon to understanding the atmosphere dynamics, as it changes temperature, pressure, density and composition. Due to exponentially decreasing density, amplitude and energy carried by these waves increase exponentially as they propagate vertically. When waves break, their energy is released, transferred to the background flow. Gravity Waves (GWs) with small horizontal wavelength can propagate up to the middle atmosphere but are too small to be resolved by most global-scale atmospheric models. The deep convection from monsoon regions is known as major source of mesospheric GWs and previous studies on summer northern hemisphere have shown that monsoon GWs tend to propagate obliquely from low-latitude stratopause up to high-latitude mesopause. We focus this study on the summer southern hemisphere and the Inter-Hemispheric Coupling (IHC) between the summer mesopause where Polar Mesospheric Clouds (PMCs) form, and the winter stratosphere where sudden warmings occur and change the IHC pattern described by previous studies. PMCs are excellent indicators of atmospheric changes and their correlations with wind, temperature and GW momentum flux highlight the consequences of anomalies in winter stratosphere, such as warmings, on the oblique propagation of GWs that influence the PMC formation in summertime southern hemisphere.

1 Introduction

The dynamics significant to the coupling between atmospheric regions involve the generation, propagation, and modulation of tides, Planetary Waves (PWs), and Gravity Waves (GWs). Of note are dynamical processes associated with GWs, since these waves are the least understood, due to the need to parameterize these waves in global climate models due to their small scales. This study contributes to the understanding of the coupling between atmospheric regions, specifically between the tropical stratosphere, a source of monsoon GWs, and high-latitude mesosphere, where Polar Mesospheric Clouds (PMCs) form (Rapp et al., 2002). Sato et al. (2009) first suggested that obliquely propagating GWs from monsoon regions can be an important source of mesospheric GWs. More recently, Thurairajah et al. (2017 & 2020) used satellite observations of PMCs and Gravity Wave Momentum Flux (GWMF) to study the effect of obliquely propagating monsoon generated GWs on PMCs in the Northern Hemisphere (NH). This work further investigates this topic focusing on the Southern Hemisphere (SH). PMCs existence result from a dynamical refrigeration process of the summer mesopause region, driven by GWs. In the winter hemisphere, Rossby waves from troposphere induce a poleward flow called Brewer–Dobson circulation. The small-scale GWs, filtered out by this stratospheric circulation, can propagate up to winter mesosphere and drive a poleward circulation that leads to an equatorward circulation in summer mesosphere. This pole-to-pole circulation implies an adiabatic expansion of the summer pole that cools the summer mesopause down enough to form PMCs (Karlsson & Shepherd, 2018). While the propagation and the breaking processes of these GWs are responsible for the cold summer mesopause, GWs have also been shown to cause the sublimation of cloud particles leading to the destruction of PMC layers (e.g. Jensen & Thomas, 1994; Rapp et al., 2002; Gerrard et al., 2004; Chandran et al., 2012; Chu et al., 2009) and enhancement of PMCs (Gao et al., 2018).

Sato et al. (2009) suggested that the largest source of mesospheric GWs in summer is the deep convection from monsoon regions. From model simulations, Sato et al. (2009) showed that the latitudinal shear in the prevailing westward jet, that has a slanted structure from the tropical stratosphere to the polar mesosphere, could refract these monsoon generated GWs to the high-altitude mesosphere. The oblique propagation (or latitudinal but vertical propagation away from the source) has been reported in model studies (e.g. Kalisch et al., 2014) and observations (e.g. Yasui et al., 2016; Thurairajah et al., 2017 & 2020). Yasui et al. (2016) used mesospheric wind data from Antarctica and precipitation data from the tropics and found that a significant component of the mesospheric GWs in high-latitude summer SH originates from tropical convection (i.e. monsoon regions). Thurairajah et al. (2017 & 2020) used data from two satellite instruments and showed a high correlation between observations of the GWMF from monsoon GWs and PMCs in summer NH. This oblique propagation of GWs, from low-latitude troposphere to high-latitude mesosphere, is not included in current gravity wave parameterization schemes but may be an important component of the global dynamical structure of the mesosphere.

Karlsson et al. (2007) found correlations between the temperature in the winter polar stratosphere and the PMC Occurrence Frequency (PMC OF) observed in the opposite summer hemisphere during Sudden Stratospheric Warmings (SSWs). SSWs are a consequence of interactions between the atmospheric PWs and the mean flow in polar stratosphere (Matsuno, 1971). During SSWs, PWs induce a reversal of the polar stratospheric jet from eastward to westward in winter hemisphere. The changes in the background wind alter the filtering of GWs

and, consequently, the directions of GWs drag from westward to eastward in the middle to high latitudes (~60-90°) (e.g. Liu et al., 2002). The resulting equatorward circulation in the upper mesosphere yields an upward flow in the mesosphere and a downward flow in the lower thermosphere, respectively resulting in an adiabatic cooling and warming (Liu et al., 2002; Cullens et al., 2015). In the Inter-Hemispheric Coupling (IHC) model presented by Körnich & Becker (2010), amplification of PWs and associated changes in GWs in the winter polar region alter the global residual circulation, changing the filtering of GWs in the summer hemisphere.

In this study, we analyze the influence of IHC mechanisms on PMCs by considering the effects of SSWs, occurring in winter stratosphere, on the dynamics of the summer SH and on the PMC activity in summer mesosphere. We investigate the combined influence of IHC and oblique propagation of monsoon GWs on PMCs using data from November to March of 2010/2011 (a no-SSW year) and 2012/2013 (a major SSW year). This paper is organized as follows. Section 2 presents the data and methods used in the derivation of GWMF, the process of locating the monsoon regions in summer SH, the calculation of PMC OF, and the process of identifying seasons with SSW events. Section 3 presents a comparison in PMC activity and GWMF activity above monsoon regions from 2008 to 2014, in both the NH and the SH. Section 3 also describes the monsoon regions in summer SH, the zonal mean zonal wind structure, the zonal mean GWMF, the correlation between PMCs and GWMF, and the IHC analysis using wind and temperature information. Section 4 contains a summary and conclusions.

2 Data and Methodology

2.1 Monsoon Convection and Gravity Waves

In this study, the location of the low-latitude source of GWs in summer SH is investigated using two parameters: the rainfall rate (i.e. precipitation) and the Outgoing Longwave Radiation (OLR). Both data have been shown to be a good proxy to estimate the strength of the monsoon convection (Wright & Gille, 2011). The Tropical Rainfall Monitoring Mission (TRMM) was designed to monitor and study tropical rainfall. It operated for 17 years, including several mission extensions, before being decommissioned in April 15, 2015. The rainfall rate data set is collected using the Dual-frequency Precipitation Radar (DPR) instrument. The DPR instrument is an electronically scanning radar, operating at 13.8 GHz that measures the 3D rainfall distribution over both land and ocean, and define the layer depth of the precipitation. The daily OLR information are collected by the National Oceanic and Atmospheric Administration (NOAA) satellite using the Advanced Very High Resolution Radiometer (AVHRR). NOAA-18 is a weather forecasting satellite run by NOAA and launched in 2005, into a sun-synchronous orbit at an altitude of 854 km above the Earth. OLR data at the top of the atmosphere are observed globally from the AVHRR instrument aboard NOAA-18. The daily raw data are converted into a standardized anomaly index. Negative OLR are indicative of enhanced convection and hence more cloud coverage. More convective activity implies higher, colder cloud tops, which emit much less infrared radiation into space.

GW variability is derived from temperature observations from the Sounding of the Atmosphere using Broadband Emission Radiometry (SABER) instrument onboard the Thermosphere Ionosphere Mesosphere Energetics and Dynamics (TIMED) satellite (Russell et al., 1999). Since 2002, the satellite TIMED is focused on the understanding of the energy

transfer into and out of the Mesosphere and Lower Thermosphere/Ionosphere (MLTI) region of the Earth's atmosphere (energetics), as well as the basic structure (i.e., pressure, temperature, and winds) that results from the energy transfer into the region (dynamics). SABER is a limb-scanning infrared radiometer that has provided global atmospheric measurements of temperature, pressure and geopotential height and trace species in the altitude range of 10-110 km. Due to the yaw cycle of TIMED, SABER can perform continuous measurements over the latitude range of 50°N-50°S. Using the version 2.0 level 2A data product, we derive the GWMF from the zonal and meridional component of the GWMF and under the mid-frequency approximation (Ern et al., 2011) as:

$$GWMF = \frac{1}{2}\rho\frac{k_h}{m}\left(\frac{g}{N}\right)^2\left(\frac{\hat{T}}{T_0}\right)^2$$

where ρ is the density of the background atmosphere, k_h is the horizontal wavenumber, m is the vertical wavenumber, g is the acceleration due to gravity, N is the Brunt Väisälä (i.e. buoyancy) frequency, T^ is the temperature amplitude (after removing the PW wavenumber 1-5 components), and T_0 is the background temperature. Note that the equation above only calculates the absolute values of GWMF (not its direction). This is because the satellite measurement track and the wave vector of the observed GW are not aligned, and therefore, the values of the horizontal wavelength will usually overestimate the true wavelength of the GW (Ern et al., 2011). Only the projection k of the horizontal wave vector can be determined, not the wave vector itself (Preusse et al., 2009). However, previous studies have shown that the above technique is reliable for GW related studies (e.g. Yamashita et al., 2013; Thurairajah et al., 2017).

The background conditions including winds and temperature are obtained from Modern-Era Retrospective Analysis for Research and Applications (MERRA-2), a NASA atmospheric reanalysis for the satellite era using the Goddard Earth Observing System Model, Version 5 (GEOS-5) with its Atmospheric Data Assimilation System (ADAS), version 5.12.4. The MERRA project focuses on historical climate analyses for a broad range of weather and climate time scales and places the NASA EOS suite of observations in a climate context. MERRA-2 data are available up to an altitude of ~77 km (~0.01 hPa). From this model, the zonal mean zonal wind speed and the zonal mean temperature have been computed to understand the IHC between the two regions.

2.2 Polar Mesospheric Clouds

PMC information is collected from the Cloud Imaging and Particle Size (CIPS) experiment on the Aeronomy of Ice in the Mesosphere (AIM) satellite (Russell et al., 1999). The version used is v05.10 level 3C (summary files) data product that provide season-long zonal averages of PMC occurrence. Since 2007, the primary goal of the AIM mission is to explore PMCs and to understand whether the clouds' ephemeral nature, and their variation over time, is related to Earth's changing climate. The mission collects data on cloud abundance, space distribution, and size of particles. CIPS is an ultraviolet imager that has provided PMC data (albedo, ice water content, occurrence frequency) in the latitude range of ~40-85° for both hemispheres (McClintock et al., 2008). To understand the seasonal variability in PMCs, we calculated the PMC OF by taking the sum of observed clouds over the total performed

observations. The PMC OF were daily averaged over the high-latitude region 65-85°N/S for the purpose of this study:

$$PMC\ OF = \frac{\sum observed\ clouds}{\sum observations}\%$$

For IHC study, Becker & Fritts (2006) and Karlsson et al. (2009) found a significant correlation between the vertical component of the Eliassen-Palm (EP) flux in the winter lower stratosphere and the temperature at the summer mesopause, but with a lag time that was altitude-dependent. Following the method used by Karlsson et al. (2009), we derived the lag times in PMC response to SSW using the PMC mean peak altitudes from Solar Occultation For Ice Experiment (SOFIE) instrument (Hervig et al., 2009) onboard AIM. AIM/SOFIE measures ice extinction profiles with a vertical resolution of ~1-2 km and the PMC peak ice extinction altitude at 3.064 μm gives us PMC altitudes along the PMC seasons.

2.3 Stratospheric Sudden Warmings

To identify SSWs, Charlton & Polvani (2007) used an algorithm that identifies SSWs based on the reversal of the zonal mean zonal wind from eastward to westward, at 60°N and at 10 hPa. In addition to this wind condition, SSW years can be grouped by major-, minor- and no-SSW using the condition of a positive zonal mean temperature gradient between 60°N and 85°N at 10 hPa (e.g. Cullens et al. ,2015). If both conditions are satisfied (westward wind and positive temperature gradient), a major SSW occurred. If one of the two conditions is satisfied, a minor SSW occurred. If none of the conditions is satisfied, no SSW occurred in the winter hemisphere for that particular year. Using the wind speed from MERRA-2, Figure 1 shows the zonal mean wind speed at 60°N from ~30 to ~80 km altitude during winter 2012/2013 (left) where a major SSW has been reported. The latter shows a clear reversal of the polar jet from eastward to westward (negative in blue) occurring between ~January 7th and ~January 28th 2013, Days Since Solstice (DSS) +17 and +38, respectively. Looking at the specific altitude of 10 hPa (~32 km), we can identify three years of SSW events from six winter seasons in NH from 2008/2009 to 2013/2014, plotted on the right panel of Figure 1. To understand the effects of SSWs on the IHC pattern and on the propagation of GWs, we select summer SH 2010/2011 (cyan line) as the no-SSW season and summer SH 2012/2013 (black line) as the major-SSW season for the comparison made in this study.

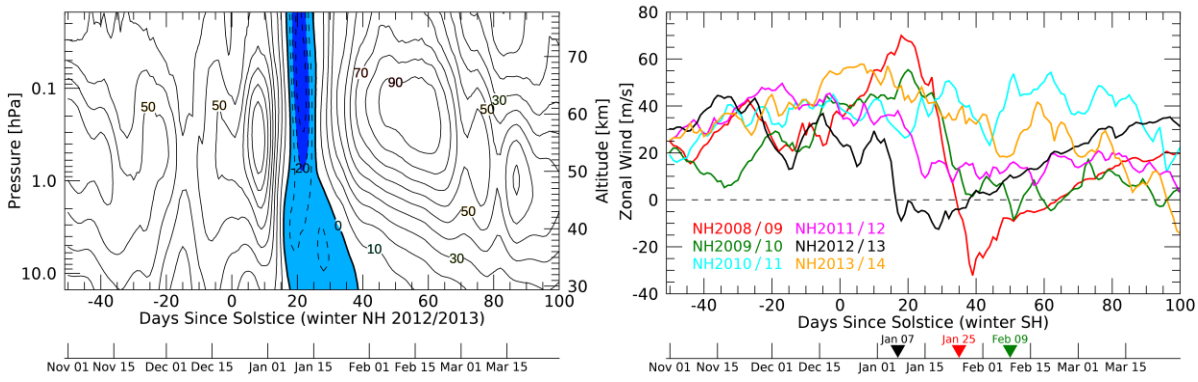

Figure 1. Zonal mean wind speed at 60°N from ~30 to ~77 km altitude during winter 2012/2013 (left) and at ~32 km (10 hPa) altitude during winter seasons from 2008/2009 to 2013/2014 (right). The wind reversal is indicated by the blue area (negative = westward) in the left panel and by the triangular markers in the right panel.

3 Results

3.1 PMC Activity

To understand the variability in the occurrence of PMCs, we use AIM/CIPS observations from years 2008 to 2014, over the summer of both hemispheres. We compute the daily-averaged PMC OF over the latitude range of ~65-85°. Figure 2 shows the PMC OF over six PMC seasons in summer NH (Figure 2.a) and six PMC seasons in summer SH (Figure 2.b) from DSS -30 to +70. For these years, one can notice the uniformity in the seasonal distribution of PMCs in summer NH compared to SH. The seasons tend to start over a 10-day window between May 21st and June 1st and end between August 20th and August 28th. The average of these six seasons (Figure 2.c) follows a normal distribution with a daily standard deviation σ ±7% in the first half and σ ±4% in the second half of the season. This consistency seen in summer NH is not present in summer SH for the same range of years. Although the PMC seasons tend to end over a 10-day window between February 11th and February 21st, the start of the PMC season varies along years (Figure 2.b). PMC seasons start either around November 21st (2009, 2012 and 2013) or around mid-December (2008, 2010 and 2011). The resulting daily standard deviation (Figure 2.d) presents an asymmetric distribution along the PMC season, from November 21st (DSS -30) to February 29th/March 1st (DSS +70), with σ ±12% in the first half and σ ±7% in the second half of the season. The peak of PMC activity for both hemispheres tends to occur ~15 days after solstice (July 6th in NH, January 5th in SH) but the amplitude of PMC OF is significantly lower in summer SH than in summer NH (~20% less PMC OF).

Looking closely at the no-SSW and major-SSW years we use for our detailed study (i.e. summer SH 2010/2011 and 2012/2013, respectively), both PMC seasons end on February 12th (DSS +53). However, while the no-SSW season SH 2010/2011 (Figure 2.b, cyan line) starts on solstice, major-SSW season SH 2012/2013 (Figure 2.b, black line) starts 25 days earlier, on November 24th (DSS -27). The average PMC OF amplitude for the major-SSW season SH 2012/2013 is also twice that of SH 2010/2011, but we observe a significant decrease from ~January 10th (DSS +20), when PMC OF is maximal, to ~January 20th (DSS +30), during 2012/2013.

PMCs in NH tend to be larger and brighter, extending to lower latitudes and exhibiting less day-to-day and year-to-year variation than their SH counterparts (Karlsson & Shepherd, 2018). Alexander & Rosenlof (1996) showed that the summer stratosphere is also warmer in the SH relative to the NH due to greater gravity wave induced forcing in the southern summer. Stratospheric hemispheric asymmetries have mesospheric counterparts whereby there would be weaker gravity wave drag in southern upper mesosphere, implying a warmer summer mesopause (Siskind et al., 2011). This has been suggested as a possible cause of the lower PMC OF in summer SH. Using the Solar Backscatter Ultraviolet (SBUV) satellite instruments, Benze et al. (2012) also found that, while the NH and SH PMC seasons on average start at the same time, variability in the SH onset date is twice as high as in the NH. Gumbel & Karlsson (2011) made

the same conclusion, using nine years of PMC observations by Odin satellite, where PMC seasons last from DSS -26 ± 3 to DSS 63 ± 3 in NH, and from DSS -24 ± 9 to DSS 58 ± 2 in SH. In addition to the confirmation of the role played by IHC from winter stratosphere on the seasonal, interannual and hemispheric variability of PMCs, Gumbel & Karlsson (2011) showed that the IHC from the summer stratosphere opens an upward pathway for polar vortex conditions to affect the summer mesosphere. Delayed start of PMC seasons can be explained by a persistent SH stratospheric jet, beyond DSS -30, and the late onset of PMC season in summer SH 2010/2011 seen in Figure 2.b coincides with a long-lasting polar vortex conditions in the Antarctic stratosphere (Gumbel & Karlsson, 2011).

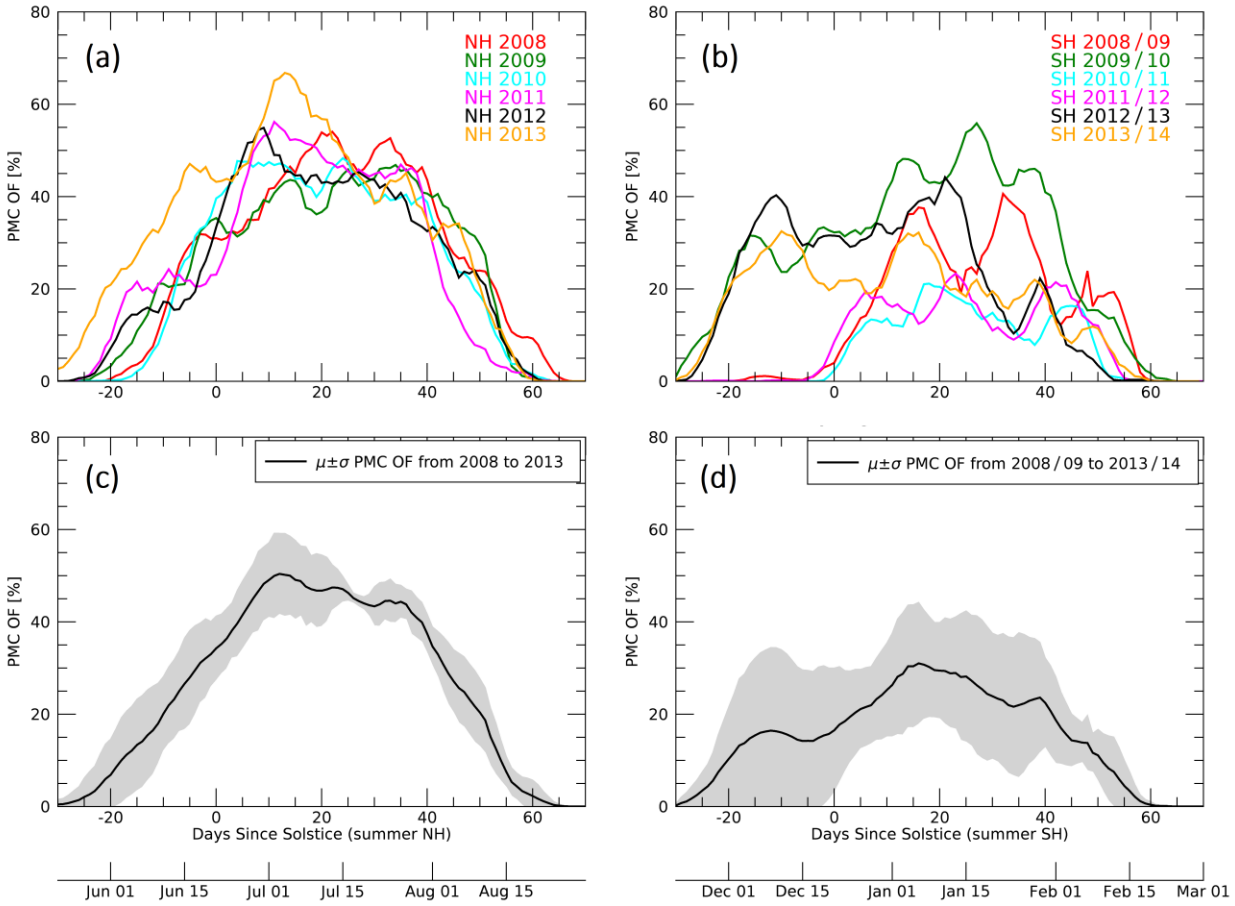

Figure 2. PMC activity in summer mesosphere using the daily-averaged PMC OF from AIM/CIPS over the ~65-85°N/S latitude band from 2008 to 2014 in summer NH (a) and summer SH (b). The mean and 1-σ standard deviation is shown in (c) and (d) for the NH and SH, respectively.

3.2 Monsoon Regions in SH

In order to locate monsoon regions in SH, we evaluate the strength of the monsoon convection by looking at the daily-averaged OLR from NOAA/AVHRR and the daily-averaged precipitation from TRMM/DPR. Figure 3 depicts both the OLR (top panel) and the precipitation

(bottom panel) for the month of January, averaged from 2008 to 2014. More convective activity implies higher, colder cloud tops, which emit much less infrared radiation into space. Therefore, a negative OLR is indicative of enhanced convection. From these two analyses, three highly convective regions have been identified in the SH: (1) Indonesia [~0-20°S, ~90°-160°E], (2) Central Africa [~0-20°S, ~15-50°E] and (3) Amazonia [~0-20°S, ~40-80°W]. The location of these regions in summer SH is consistent for individual years (not shown here) and agrees with the results obtained by Wright & Gille (2011), using the High Resolution Dynamics Limb Sounder (HIRDLS) onboard the NASA's Aura satellite (see Figure 2 and Table 1 in Wright & Gille, 2011). A parallel study on summer NH also showed the ~0-20°N latitude bin to be the most convective zonal area and a consistent monsoon region for the summer NH (not shown here).

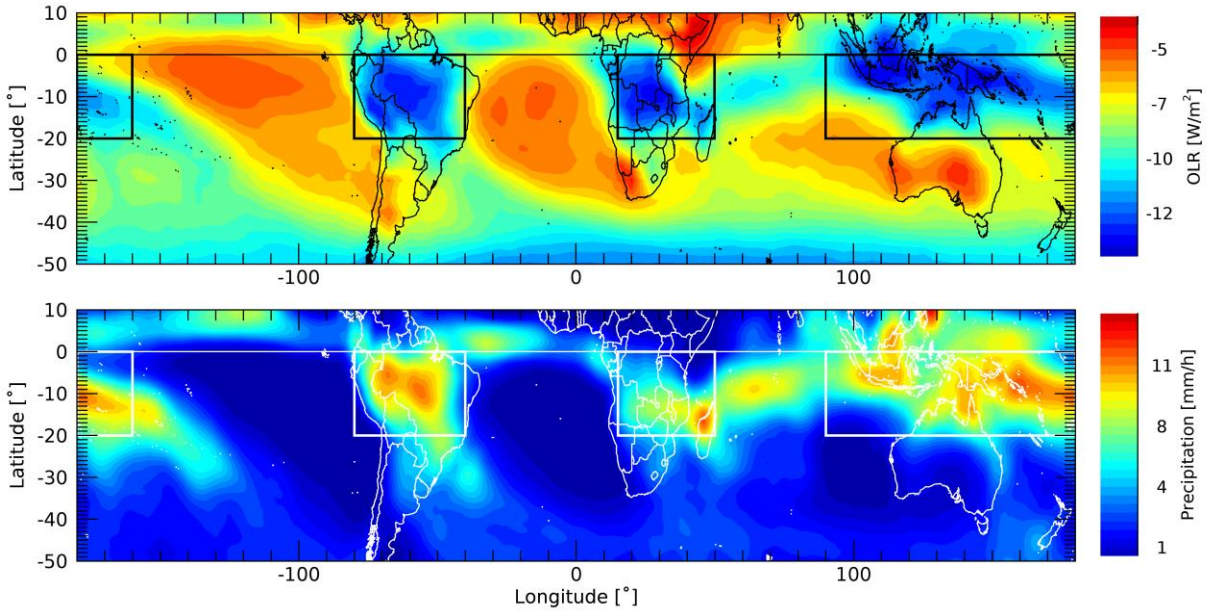

Figure 3. Daily-averaged OLR (top) from NOAA/AVHRR and daily-averaged precipitation (bottom) from TRMM/DPR in summer SH averaged over January from 2008 to 2014. Three monsoon regions: Indonesia, Central Africa and Amazonia are identified by boxes.

3.3 GWMF and Background Winds

TIMED/SABER performs continuous measurements over the latitude range of 50°N-50°S, which covers the monsoon regions. Due to the yaw cycle of TIMED, SABER observes the high-latitudes only for about half the PMC season. In the summer hemisphere, monsoon generated GWs have been shown to vertically propagate from their source in troposphere up to the stratopause (~50 km) where they focus into the mesospheric jet and can obliquely propagate to the high-latitude mesosphere (e.g. Sato et al., 2009; Thurairajah et al., 2017). Looking at 50 km above the monsoon regions (0-20°N/S) for both hemispheres, we explore the seasonal variability in the zonal mean GWMF from DSS -30 to DSS +70 in summer NH (Figure 4.a) and summer SH (Figure 4.b) for years 2008 to 2014. Figure 4.c and Figure 4.d show the corresponding average and 1-sigma standard deviation of the six seasons in summer NH and

summer SH, respectively. In both hemispheres, the momentum flux carried by GWs tends to increase until it reaches its maximum ~50 days after solstice. Note that, like the daily-averaged PMC OF (Figure 2.d), the daily standard deviation of GWMF above monsoon regions in SH (Figure 4.d) exhibits an asymmetric distribution with a distinct transition at solstice from large (σ~0.09 $\log_{10}$ hPa at DSS -5) to small (σ~0.02 $\log_{10}$ hPa at DSS +5) standard deviation. Despite this asymmetric pattern, both hemispheres present a relatively similar GWMF activity at the stratopause above their respective monsoon regions. Although monsoon regions in the widely studied summer NH present high momentum fluxes, the amplitude of GWMF above monsoon regions in summer SH is of equal if not higher than its NH counterpart for the same range of years and latitudes, consistent with results from Wright & Gille (2011).

Looking closely at the no-SSW and major-SSW years that we focus on in the next sections (i.e. SH 2010/2011 and SH 2012/2013, respectively), both years exhibit a similar GWMF seasonal distribution. The no-SSW season SH 2010/2011 (Figure 4.b, cyan line) presents a slightly higher GWMF (+0.1 $\log_{10}$ hPa) than the major-SSW season SH 2012/2013 (Figure 4.b, black line) between DSS -30 and -10 and between DSS +50 and +60.

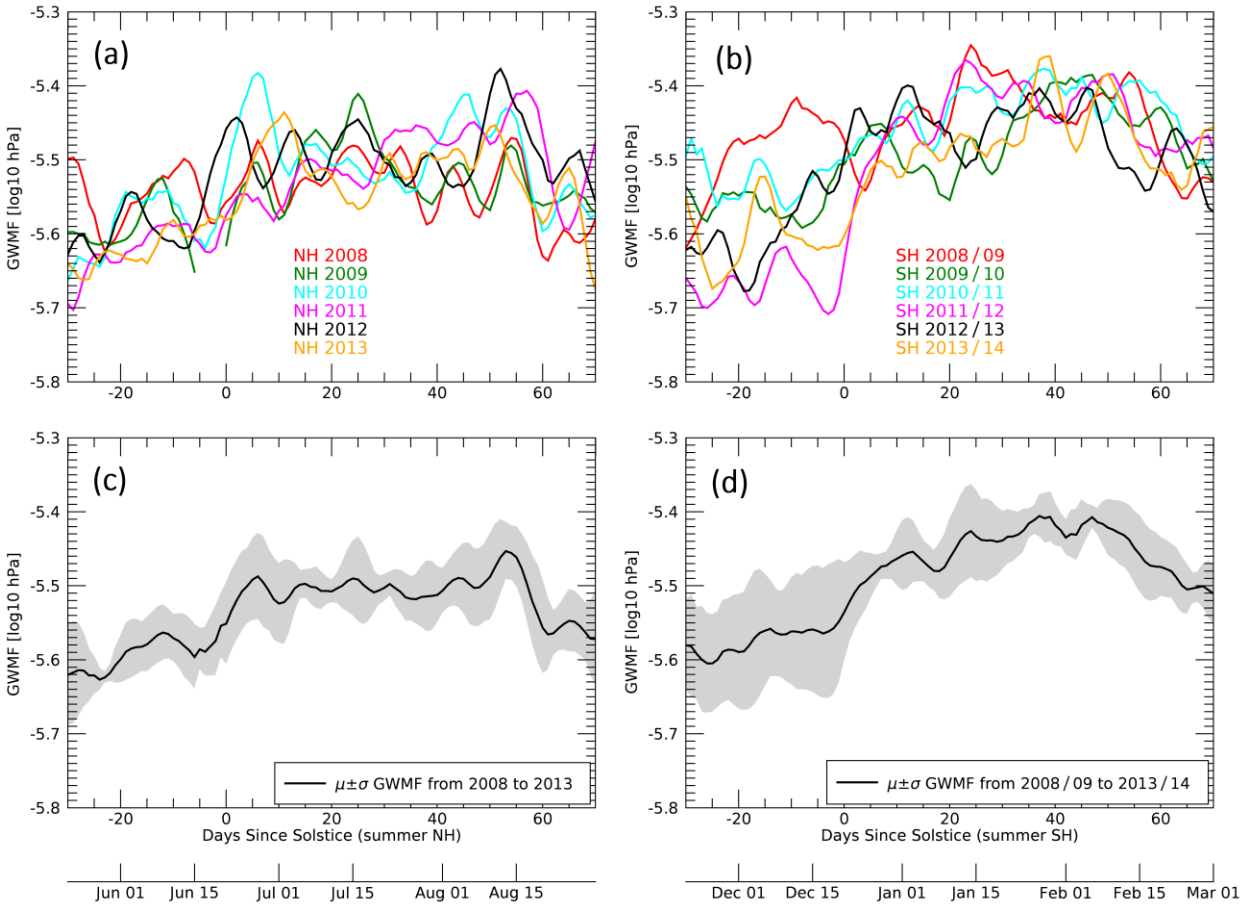

Figure 4. GW seasonal variability in summer stratopause using the daily-averaged zonal mean GWMF from TIMED/SABER above the monsoon regions (latitude ~0-20°N/S) and at ~50 km altitude from 2008 to 2014 in summer NH (a) and summer SH (b). The mean and 1-σ standard deviation is shown in (c) and (d) for the NH and SH, respectively.

In order to investigate the effects of SSWs on the GWMF, we show the superposition of the zonal mean zonal wind speed from MERRA-2 on the zonal mean GWMF for the no-SSW year 2010/2011 and the major-SSW year 2012/2013, respectively in Figure 5.a and Figure 5.b. Both data are averaged for a 21-day period, starting on January 7th when SSW triggered in winter NH 2012/2013 (see Figure 1) and ending on January 27th, 20 days after the SSW. The altitude range for the zonal wind is limited to ~30-77 km by the model's limits and the latitude range for GWMF is limited to ~50°S-85°N due to TIMED's yaw cycle during this 20-day period. The maximum GWMF, calculated at each 1-km altitude step, depicts the GW propagation in summer SH (white dots) and in winter NH (black dots). Figure 5.c shows the subtraction of the GWMF in no-SSW season 2010/2011 (Figure 5.a) from the GWMF in major-SSW season 2012/2013 (Figure 5.b). In this difference plot, a positive [negative] value indicates an increase [decrease] in GWMF during the 20 days after SSW triggered in high-latitude winter NH.

In the winter hemisphere, the stratospheric eastward jet that prevails in high latitudes (~60-90°) can be attributed to the polar vortex, which is an important source of GWs (Ern et al., 2011). When no SSW is reported (e.g. winter NH 2010/2011, Figure 5.a), maximum GWMF in winter NH depicts the vertically propagating GWs in polar vortex at high latitudes (~70°N) and up to ~65 km altitude, following the strong eastward wind (> 50 m/s). When a major SSW occurs (e.g. winter NH 2012/2013, Figure 5.b), a reversal of the polar stratospheric jet is observed between latitudes ~55-85°N at 10 hPa altitude which reduces the strength of the eastward jet in winter tropical NH (< 30 m/s). The poleward flow (i.e. Brewer–Dobson circulation) at this altitude is strongly enhanced and, as a result of the so-induced warmer temperature and weaker eastward zonal wind, the westward GWs break at lower altitudes (Becker, 2012). The GWMF in the high-latitude winter stratosphere and winter mesosphere is therefore lower compared to the no-SSW winter NH (Figure 5.c). The reduction of ~0.5 $\log_{10}$ hPa at approximately 55 km altitude and 75°N corresponds to a 68% decrease in GWMF (hPa). This reduced GW activity associated with SSW has been reported in previous studies (e.g. Siskind et al., 2010). The GWMF maximum at each altitude step no longer presents as a vertical pattern as seen for 2010/2011 (Figure 5.a) but is at mid latitudes (~50°N) and slanted toward the equator as altitude increases, following the weaker stratospheric eastward jet (Figure 5.b). Figure 5.c also shows this increase in GWMF of almost 100% (+0.3 $\log_{10}$ hPa) from tropical winter stratosphere (~30 km altitude, ~50°N latitude) and along the same equatorward pattern described previously.

Above the monsoon regions (latitudes ~0-20°S), GW propagation is quasi vertical up to the stratopause (~50 km). As the GWs propagate vertically, the GWMF decreases with altitude due to dissipation, they decelerate the jet and contribute to the slanted structure of the westward wind (Sato, et al., 2009). This westward wind associated with the monsoon circulation is slanted toward the high latitudes and allows the oblique propagation of the GWs generated from the low-latitude monsoon regions to the high-latitude mesosphere. The structure of the westward wind, slanted toward the summer pole and the mesospheric altitudes, is consistent for all years from 2008 to 2014 (not shown here). In response to the SSW event and for the 20 days that follow, the

summer SH sees a significant increase in GWMF concentrated at ~30 km altitude above equator (Figure 5.c) of about 82% (+0.26 $\log_{10}$ hPa). Although the path depicted by the maximum GWMF (white dots) remains similar between summer SH 2010/2011 and summer SH 2012/2013 (Figure 5.a and 5.b, respectively), we observe an increase of between 7% and 17% (+0.03 and +0.07 $\log_{10}$ hPa) in GWMF over a larger region, from ~30 km to ~80 km altitude and above the latitude bin ~30-50°S (Figure 5.c), but the path depicted by the maximum GWMF (white dots) remains similar between summer SH 2010/2011 and summer SH 2012/2013 (Figure 5.a and 5.b, respectively).

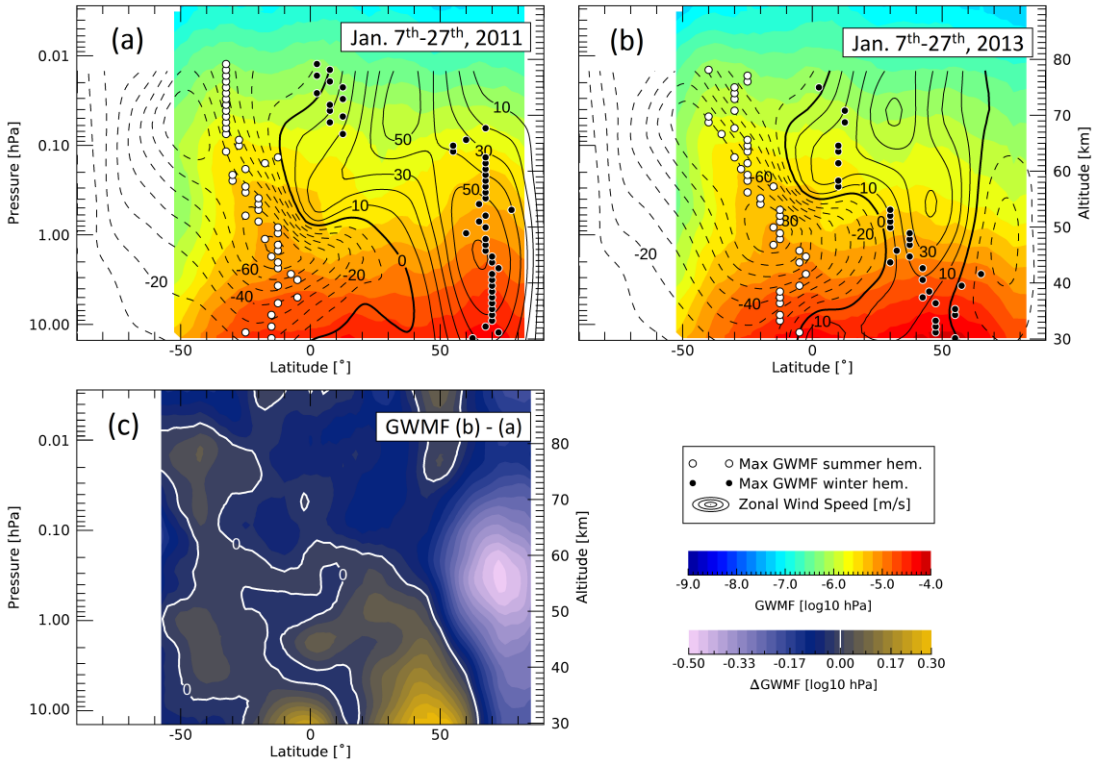

Figure 5. Zonal mean GWMF from TIMED/SABER (color) and zonal mean zonal wind speed from MERRA-2 (solid lines for eastward, dashed lines for westward) averaged from January 7th to January 27th in (a) 2011 and (b) 2013. GWMF maxima at each 1-km step altitude are depicted by white and black dots, respectively in summer SH and winter NH. (c) Difference in GWMF between no-SSW and major-SSW seasons by subtracting GWMF in (a) from GWMF in (b).

3.4 Correlation between PMCs and GWMF

Obliquely propagating GWs generated from low latitudes have been shown to have an influence on the polar summer mesosphere (Thurairajah et al., 2017 & 2020) and PMCs are sensitive indicators of such changes (Karlsson & Shepherd, 2018). While Thurairajah et al., (2017 & 2020) presented results in the summer NH, here we study the instantaneous correlation between the time series of PMC OF in southern summer upper mesosphere (latitudes ~65-85°S) and GWMF measured over the latitude range 50°S-50°N and the altitude range 30-90 km. Figure

6.a and Figure 6.b depict the correlation coefficients, for 2010/2011 (no-SSW) and 2012/2013 (major-SSW), respectively, using data from November 21st (DSS -30) to March 1st (DSS +70).

In both seasons, the high-correlated region ($r > 0.5$) in mid-latitude summer mesosphere is assumed (based on Figure 5) to be associated to the oblique propagation of GWs above monsoon regions in low-latitude stratopause and slanted poleward to high-latitude mesopause. We also observe a positive correlation in the winter hemisphere at lower altitudes that confirms the link between the wintertime dynamics and the summer mesopause in the opposite hemisphere. A positive correlation between PMC OF and GWMF means that an increase in GW activity correlates with an increase in PMCs activity, and vice-versa.

When SSWs occur in winter stratosphere, the small region of high correlation ($r > 0.5$) between PMCs and GWMF in winter stratopause (~50 km altitude, ~32°N latitude) seen in Figure 6.a for the no-SSW year is replaced by a significantly larger area (~30-60 km altitude, ~30-50°N latitude) of high correlation (Figure 6.b). It exhibits the same pattern seen in the GWMF maxima (Figure 5.b, black dots) and GWMF difference between no-SSW and major-SSW (Figure 5.c), starting at mid latitudes and slanted toward the equator as altitude increases. This suggests that, although the GW activity in winter stratosphere is strongly reduced during SSW events, with breaking occurring at lower altitudes, the PMC seasonal variations is more correlated with the GWMF variations associated with the SSW dynamics. It demonstrates the impact of winter GWs on the global mean meridional circulation and the summer mesopause cooling (Karlsson & Becker, 2016).

The high-correlated region ($r > 0.5$) in mid-latitude summer mesosphere is replaced by a larger area with higher coefficients when major SSW occur in summer SH 2012/2013 (Figure 6.b). If we evaluate the angle of this high correlation structure using a hypothetical straight line slanted poleward, the resulting straight line stays in summer SH for the no-SSW season (Figure 6.a), connecting the low-latitude summer stratosphere (~30 km altitude, ~10°S latitude) with mid-latitude mesopause (~80 km altitude, ~30°S). However, the same method in Figure 6.b exhibits a diagonal line that connects the mid-latitude winter stratosphere (~30 km altitude, ~50°N) with the mid-latitude summer mesosphere (~80 km altitude, ~40°S latitude). This diagonal of positive correlations between PMCs and GWMF is between two large highly anti-correlated regions ($r < 0.5$): the equatorial upper mesosphere (~75 km altitude, ~0° latitude) and the low-latitude upper stratosphere (~50 km altitude, ~20-40°S latitude). These observations suggest that, despite a similar zonal mean westward wind structure prevailing in summer SH for a 20-day period between 2010/2011 and 2012/2013 (see Figure 5.a and 5.b), the major SSW, occurring in winter stratosphere, changes GW activities in the SH. For the no-SSW season (e.g. summer SH 2010/2011), the GWs from monsoon convection that are presumed to propagate vertically and reach ~50 km altitude, then obliquely propagate following the poleward tilt of the easterly jet that prevails in summer SH. This agrees with the results obtained in summer NH by Thurairajah et al. (2017). For the major-SSW season (e.g. summer SH 2012/2013), the oblique propagation of monsoon GWs appears to be modified by the dynamics associated with the SSW in the NH winter. The high correlation region, above monsoon regions, is at a higher altitude above the stratopause (~65 km) and slanted poleward with a sharper angle in mesosphere.

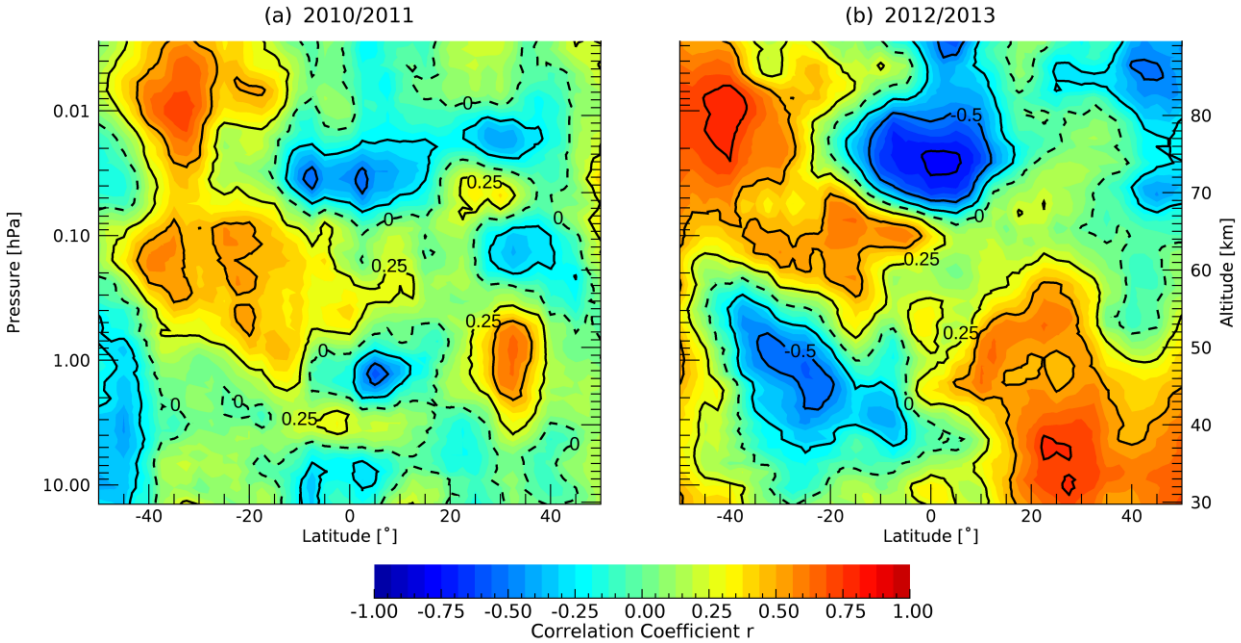

Figure 6. Correlation coefficient between time series of PMC OF, observed by AIM/CIPS from southern summer mesopause (~84 km altitude, ~65-85°S latitude), and GWMF from TIMED/SABER over the meridional cross section (~30-90 km altitudes, ~50°S-50°N latitudes), daily-averaged from DSS -30 to DSS +70 in (a) summer SH 2010/2011 and (b) summer SH 2012/2013. Dashed lines denote the 0 and solid lines denote the ±0.25, ±0.5 and ±0.75 correlation coefficients (r).

3.5 IHC analysis

Due to the yaw cycle of TIMED, no GWMF information is available in the high-latitude summer SH from January ~15th to March ~15th, when SSWs usually occur in the opposite winter stratosphere (see Figure 5). Therefore, we investigate the effect of SSWs on the PMC region by comparing summer SH 2010/2011 (no-SSW) with summer SH 2012/2013 (major-SSW) within an IHC analysis, applying the method used by Karlsson et al. (2009) and graphically described by Figure 7. Here we use the zonal mean zonal wind (U) and the temperature (T) from MERRA-2, in the available altitude range (~0-77 km). Although the top altitude does not include the PMC altitudes, we can have a sense of change in U and T seen in IHC mechanism.

Following Karlsson et al. (2009), we first compare the PMC OF, averaged over latitudes 65-85°S, with the zonal mean zonal wind, averaged over latitudes 59-61°N and altitudes 10-5 hPa. At ~60°N, this altitude region is a good indicator of the variability in the winter stratosphere (Karlsson et al., 2009). Figure 7.a shows the PMC OF from AIM/CIPS for SH 2010/2011. Since the IHC of the middle atmosphere general circulation is characterized by a global anomaly pattern of the zonal mean temperature, this analysis uses the anomaly fields of PMCs, wind and temperature data ($\overline{PMC\ OF'}$, $\overline{U'}$ and $\overline{T'}$, respectively) which we derive by subtracting the 6th-order polynomial fitting of the data from the data itself. Figure 7.b shows SH $\overline{PMC\ OF'}$ and NH $\overline{U'}$ for 2010/2011. By computing a time-lagged correlation between these two parameters, the highest correlation coefficient indicates two lag times. There is a 9-day lag in the first half of the

PMC season, and a 13-day lag in the second half of the PMC season. Halves of the PMC season are indicated by the dashed vertical lines in Figure 7. Karlsson et al. (2009) noted that the lag changes during the PMC season due to the associated change in PMC altitudes. Therefore, the resulting lag times are altitude-dependent. In Figure 7.c we show the PMC altitudes from AIM/SOFIE data. Using a linear fit of the PMC altitude variations, the two lag times are then used as two points on DSS +14 and +40 (i.e the median dates) to obtain an interpolated time varying lag along the PMC season.

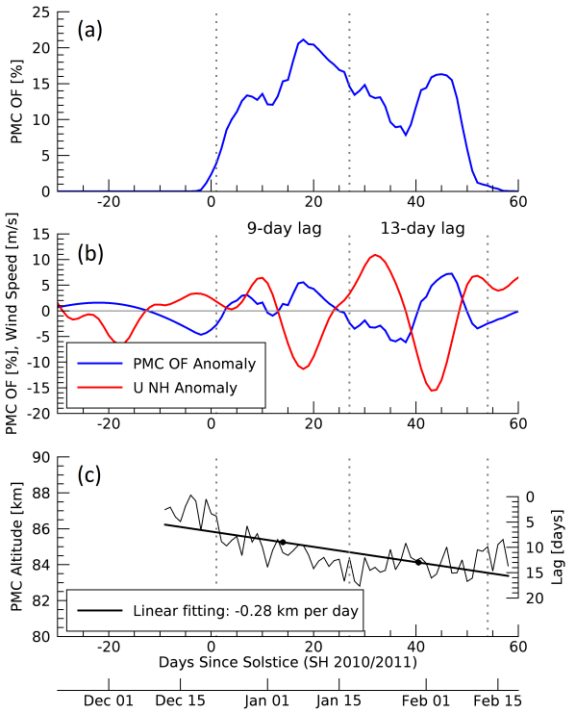

Figure 7. (a) PMC OF from AIM/CIPS averaged over latitudes 65-85°S for SH 2010/2011, (b) anomaly fields of the PMC OF (blue) and the zonal mean zonal wind from MERRA-2, averaged over latitudes 59-61°N and altitudes 10-5 hPa (red), seen from November 21st to February 19th. (c) PMC altitudes from AIM/SOFIE. The linear fit is shown by the straight line.

From this method, we compare the correlation of PMC OF anomaly with the global zonal mean zonal wind and the zonal mean temperature anomaly fields from MERRA-2 for both summer SH 2010/2011 and summer SH 2012/2013 (see Figure 8 and 9, respectively). This correlation analysis is focused on data from November 21st (DSS -30) to March 1st (DSS +70).

In Figures 8.a and 9.a, both the no-SSW and the major-SSW seasons show large areas of high correlation (r > 0.5) between $\overline{PMC\ OF'}$ and $\overline{U'}$. The area with strongest coefficients is located in the winter stratosphere, highly correlated with PMCs in summer mesopause and agreeing with IHC mechanism described by Karlsson et al. (2009). The second area of positive correlation between $\overline{PMC\ OF'}$ and $\overline{U'}$ is located in the opposite summer stratosphere and is due to dynamics in the winter stratosphere affecting the summer stratospheric flow. During SSW, these two positive correlation areas are enhanced (Figure 9.a) and the higher correlation with the eastward $\overline{U'}$, prevailing in high-latitude winter NH and weakened by SSW, suggests that PMC

day-to-day variations are significantly more correlated with anomalies caused by SSW that cross the equator via the meridional circulation.

In Figures 8.b and 9.b, both the no-SSW and the major-SSW seasons show a negative correlation between $\overline{PMC\ OF'}$ and $\overline{T}'$ in high-latitude winter stratosphere associated with a positive correlation in equatorial stratosphere and a positive correlation in polar winter mesosphere. This quadrupole structure agrees with previous IHC analyses. Karlsson et al. (2007) showed this positive/negative winter dipole pattern in the correlation between noctilucent cloud properties and stratospheric temperatures in winter stratosphere from July 2002 to January 2007. Due to higher PW activity in winter troposphere and stratosphere, high-latitude stratosphere and low-latitude mesosphere experience warming while high-latitude mesosphere and low-latitude stratosphere experience cooling. The deceleration of the zonal wind by PWs leads to a reduction of the net GW drag, responsible for driving the mesospheric meridional circulation (Becker & Fritts, 2006). The winter mesospheric meridional circulation being weaker, the high-latitude adiabatic heating is reduced and the high-latitude winter mesosphere is cooler during high PW activity. It also reduces the upwelling and increases temperature in equatorial mesosphere. In stratospheric altitudes, the Brewer-Dobson circulation warms the high latitudes up and cools the equatorial stratosphere down.In both seasons, the correlation between $\overline{PMC\ OF'}$ and $\overline{T}'$ tend to exhibit this quadrupole structure in winter hemisphere. However, the most important step for IHC consists of how anomalies, induced by SSWs, cross the equator. As the zonal wind does not change in summer stratosphere, the GW filtering remains the same between no-SSW and major-SSW season, and it allows large phase speed GWs to propagate up to mesosphere. In this region, the $\overline{U'}$ anomaly makes the background wind closer to the GW phase speed and induces wave breaking at lower altitudes, creating a downward shift of the GW drag associated with a downward shift of the upper branch of the residual circulation (Körnich & Becker, 2010). This leads to a positive $\overline{T}'$ anomaly in summer polar mesopause during SSWs.

In addition to a strongly enhanced quadrupole structure in major-SSW season 2012/2013, we observe a strong positive correlation between $\overline{PMC\ OF'}$ and $\overline{T}'$ below the PMC region in Figure 9.b. This high-correlation area, concentrated only in the equatorial stratosphere for SH 2010/2011 (Figure 8.b), extends towards high-latitude summer mesosphere for SH 2012/2013, depicting a pattern slanted poleward from low-latitude stratopause to high-latitude mesosphere (Figure 9.b). Knowing that a positive correlation with temperature can be associated to the destruction of PMC layers (Gumbel & Karlsson, 2011), this correlation using the adjusted-lag PMC OF explains the decrease in PMC OF occurring later in SH 2012/2013 season at DSS +20 (see Figure 2.b). Siskind et al. (2011) have shown that a similar decrease in PMC activity at mid-season NH 2007 likely resulted from IHC due to enhanced PWs in the SH winter. Karlsson & Becker (2016) showed that winter GW activity reduces the net GW drag in the winter mesosphere, which then leads to a weaker winter residual circulation and a warmer summer polar mesosphere. The change in dynamics, induced by the major SSW and associated with the temperature patterns in Figure 8.b and 9.b, could also explain the change in the correlation pattern between PMC OF and GWMF in Figure 6.a and 6.b.

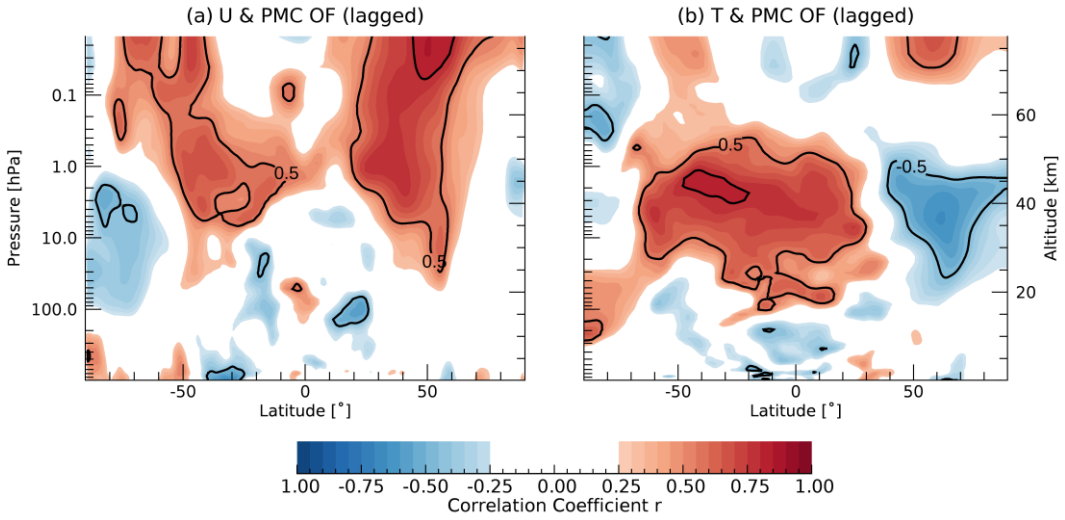

Figure 8. Correlation coefficients of the lag-adjusted PMC OF anomaly with (a) the zonal mean zonal wind speed $\overline{U'}$ and with (b) the zonal mean temperature $\overline{T}'$ from MERRA-2, for summer SH 2010/2011 (no SSW). Black contours denote the ±0.5 and ±0.75 correlation coefficients (r).

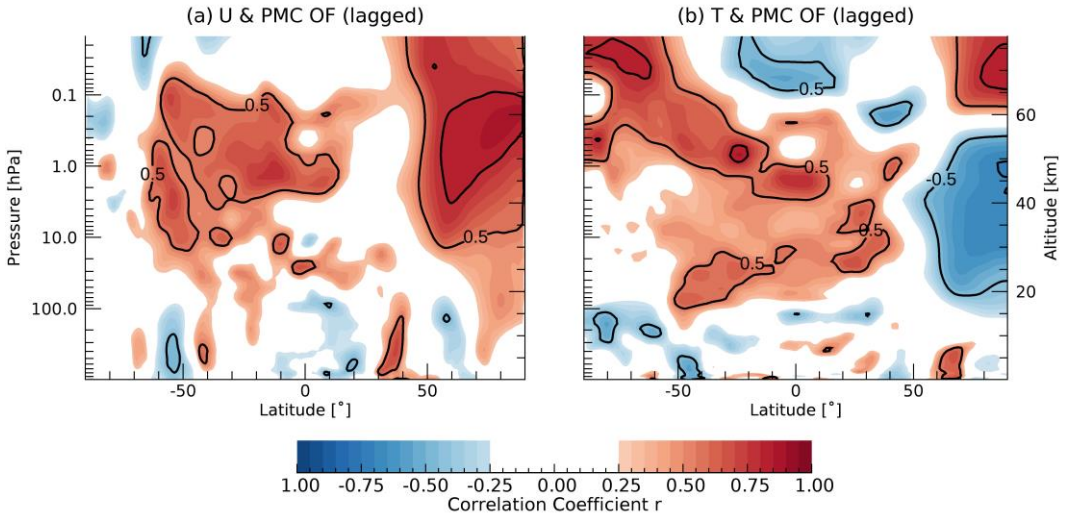

Figure 9. Same as Figure 8 but for summer SH 2012/2013 (major SSW).

4 Summary and conclusions

Oblique propagation of GWs refers to the latitudinal propagation of GWs, from the summer stratosphere above the tropical monsoon convection source to the high-latitude summer mesosphere. Previous studies have been conducted in summer NH using a large range of PMC seasons and revealed a high correlation between observations of the GWMF from monsoon GWs and PMCs. Although this oblique propagation plays an important role in the global dynamical structure of the mesosphere, it is not included in GW parameterization schemes. Motivated by these studies, here we presented a combination of satellite observations and model to understand this atmospheric phenomenon in the summer SH. We compared six PMC seasons in summer NH and six PMC seasons in summer SH from 2008 to 2014. PMC OF in summer NH tends to

exhibit a normal distribution from DSS -30 to +70 but this consistency and symmetry was not present in the PMC OF in summer SH. PMCs in NH tend to be larger and brighter, extending to lower latitudes and exhibiting less day-to-day and year-to-year variation than their SH counterparts (Karlsson & Shepherd, 2018).

Knowing the largest source of GWs in summer troposphere to be the deep convection from monsoon regions (Sato et al., 2009), we measured the convection strength in summer SH. We identified three high-convective regions: (1) Indonesia [~0-20°S, ~90°E-160°E], (2) Central Africa [~0-20°S, ~15-50°E] and (3) Amazonia [~0-20°S, ~40-80°W]. We then analyzed the daily-averaged zonal mean GWMF above these regions for both hemispheres from 2008 to 2014. Despite an asymmetric distribution in SH, which was also present in the daily-averaged PMC OF, GWMF amplitudes above monsoon regions in SH is as significant as its widely more studied NH counterparts are.

In addition to this hemispheric comparison, we were interested in the effects of the seasonal variability in the opposite winter NH. We identified years when SSWs (major and minor) occurred by looking at the polar jet reversal (from eastward to westward) at 60°N latitude and ~32 km (10 hPa) altitude using MERRA-2 winds. As a case of study, we focused the rest of our analysis on two PMC seasons in SH, 2010/2011 (no SSW was observed in the NH) and 2012/2013 (major SSW occurred in the NH). We then compared the zonal mean GWMF and the zonal mean zonal wind speed between the two PMC seasons, averaged for 21 days starting on January 7th, when major SSW occurred in 2013. For no-SSW year (2010/2011), results confirmed the vertical propagation of GWs from polar vortex, focusing into the strong stratospheric eastward jet. In addition, oblique propagation of GWs from the southern monsoon regions to the southern mesosphere are shown, consistent with previous work on oblique propagation of GW in the NH. During the SSW in 2013, the eastward jet in winter NH is reversed to westward, and westward GWs tend to break at lower altitudes. The resulting lower GW activity in high-latitude stratosphere is shown by a 68% decrease in GWMF (-0.5 $\log_{10}$ hPa), at ~55 km and ~75°N, compared to the no-SSW year. This decrease is counter-balanced by a significant increase in GWMF (+0.3 $\log_{10}$ hPa, +100% hPa) at ~30 km and ~50°N. As a result, the maximum GWMF located at mid latitudes in stratosphere and slanted toward equator as altitude increases, following the weaker stratospheric eastward jet. Although the oblique propagation of GWs from southern monsoon regions, depicted by the maximum GWMF, is seen in both seasons (no-SSW and major-SSW), the GWMF at ~30 km above equator is shown to be 82% greater (+0.26 $\log_{10}$ hPa) in major-SSW season than in no-SSW season. This increase in GWMF extended from ~30 km to ~80 km altitude and above the latitude bin ~30-50°S, between 7% and 17% greater (+0.03 and +0.07 $\log_{10}$ hPa) in major-SSW season than in no-SSW season.

By investigating the correlation between daily-averaged PMC OF and zonal mean GWMF, three observations can be made regarding the effects of SSW. (1) Although the GWMF contribution in winter stratosphere is strongly reduced during SSWs, the PMC seasonal variations in the summer SH is highly correlated with these GWMF seasonal variations in NH. (2) This high-correlated region also exhibits the same pattern seen in the GWMF maxima (Figure 5.b, black dots), located at mid latitudes and slanted toward the equator as altitude increases, following the weaker stratospheric eastward jet. (3) Despite a similar westward zonal wind structure in summer SH between both seasons, the major SSW changes the high-correlation structure of PMC OF – GWMF in summer mesosphere, which was associated to the propagation of monsoon generated GWs. The major-SSW summer SH 2012/2013 shows a pattern that starts

at higher altitude (~65 km) and is slanted poleward with a sharper angle in mesosphere, compared to the oblique propagation described by Thurairajah et al. (2017) and shown in the no-SSW summer SH 2010/2011.

Extending this study beyond the range of SABER at higher latitudes, we performed the IHC analysis following the method used by Karlsson et al. (2009), investigating the correlation of the day-to-day variability in PMC OF with the variability in the zonal mean zonal wind and temperature from MERRA-2. The comparison of both seasons showed agreements with the IHC mechanisms described in previous studies (Karlsson et al., 2007 ; 2009 ; 2016) and highlighted the influence of major SSWs in winter NH on PMCs in summer SH. The results obtained in summer SH 2012/2013 are similar to results obtained by Karlsson et al. (2009) in summer SH 2007/2008, where major SSW has also been reported. (1) The strong correlation of adjusted-lag $\overline{PMC\ OF'}$ with high-latitude stratospheric wind $\overline{U'}$ is largly enhanced for major-SSW season (|r| +14%), suggesting that the day-to-day variability in PMCs is more correlated to SSW-induced anomalies that cross the equator via the meridional circulation. (2) The quadrupole structure of correlation and anti-correlation between $\overline{PMC\ OF'}$ and $\overline{T}'$ is significantly enhanced for the major-SSW season, presenting a higher absolute value of the correlation coefficient when major SSWs occur (|r| +21%). This suggests that the day-to-day PMC variability in summer SH is significantly more correlated to variabilities in $\overline{U'}$ and $\overline{T}'$ during SSW events. (3) The positive correlation between $\overline{PMC\ OF'}$ and $\overline{T}'$, depicted by a large structure slanted poleward from equatorial stratosphere to high-latitude summer mesosphere for SH 2012/2013, could explain the decrease seen in PMC OF for the same season, occurring later at DSS +20. Although the permanent effect of IHC is a cooling of the high-latitude summer mesosphere, shown by Karlsson & Becker (2016) to be determined by the strength of the westward GW drag in the winter mesosphere, the increased GW activity in winter stratosphere can leads to a warmer summer polar mesosphere via a weaker residual circulation (Karlsson & Becker, 2016).

In conclusion, we showed that the major SSW in winter NH 2012/2013 increases the GWMF in summer SH, enhances the correlation between PMCs and GWs which are assumed to be from monsoon regions, and changes the dynamics of the global atmosphere. We also showed, by using the adjusted-lag PMC OF, that major SSWs can play a role in the destruction of PMC layers, days later in the PMC season. While the intra-hemispheric connection between low- to high- altitude summer hemisphere has been shown to influence the start of PMC season due to the persistency of the polar vortex (Gumbel and Karlsson, 2011), this study showed enhancement in IHC between winter stratosphere in NH and summer stratosphere in SH during SSWs, that in turn reduces the seasonal PMC activity. We expect to verify these observations regarding the effects of SSWs on GW propagation from troposphere in both hemispheres, in the future, using ray-tracing simulations.

Acknowledgments and Data

The TIMED/SABER data (version 2.0 level 2A) are available from the SABER website (http://saber.gats-inc.com/data.php). The precipitation data from TRMM/DPR are available from NASA's Data and Information Services Center website (https://disc.gsfc.nasa.gov/datasets/TRMM_3B42_Daily_7/summary). The radiation data from NOAA/AVHRR are available from NOAA's Physical Sciences Laboratory website (https://psl.noaa.gov/data/gridded/data.uninterp_OLR.html#plot). MERRA-2 simulations

(version 5.12.4) are available from NASA's Data and Information Services Center website (https://disc.gsfc.nasa.gov/datasets/M2I6NVANA_5.12.4/summary). The PMC data from AIM/CIPS are available from the Laboratory for Atmospheric and Space Physics website (http://lasp.colorado.edu/aim/download-data-L3C.php) and PMC data from AIM/SOFIE are available from the SOFIE website (http://sofie.gats-inc.com/sofie/index.php). This research was supported by NASA Grant 80NSSC18K0650 and by NSF award 1855476.

References

Alexander, M. J., & Rosenlof, K. H. (1996). Nonstationary gravity wave forcing of the stratospheric zonal mean wind. *Journal of Geophysical Research: Atmospheres*, 101(D18), 23465-23474.

Becker, E. (2004). Direct heating rates associated with gravity wave saturation. *Journal of atmospheric and solar-terrestrial physics, 66(6-9), 683-696.*

Becker, E. (2012). Dynamical control of the middle atmosphere. *Space science reviews*, 168(1-4), 283-314.

Becker, E., & Fritts, D. C. (2006). Enhanced gravity-wave activity and interhemispheric coupling during the MaCWAVE/MIDAS northern summer program 2002.

Benze, S., Randall, C. E., Karlsson, B., Harvey, V. L., DeLand, M. T., Thomas, G. E., & Shettle, E. P. (2012). On the onset of polar mesospheric cloud seasons as observed by SBUV. *Journal of Geophysical Research: Atmospheres, 117(D7).*

Chandran, A., Rusch, D. W., Thomas, G. E., Palo, S. E., Baumgarten, G., Jensen, E. J., & Merkel, A. W. (2012). Atmospheric gravity wave effects on polar mesospheric clouds: A comparison of numerical simulations from CARMA 2D with AIM observations. *Journal of Geophysical Research: Atmospheres, 117(D20).*

Charlton, A. J., & Polvani, L. M. (2007). A new look at stratospheric sudden warmings. Part I: Climatology and modeling benchmarks. *Journal of Climate, 20(3),* 449-469.

Chu, X., Yamashita, C., Espy, P. J., Nott, G. J., Jensen, E. J., Liu, H. L., & Thayer, J. P. (2009). Responses of polar mesospheric cloud brightness to stratospheric gravity waves at the South Pole and Rothera, Antarctica. *Journal of atmospheric and solar-terrestrial physics, 71(3-4),* 434-445.

Cullens, C. Y., England, S. L., & Immel, T. J. (2015). Global responses of gravity waves to planetary waves during stratospheric sudden warming observed by SABER. *Journal of Geophysical Research: Atmospheres*, 12-18.

Ern, M., Preusse, P., Gille, J., Hepplewhite, C., Mlynczak, M., Russell, J., & Riese, M. (2011). Implications for atmospheric dynamics derived from global observations of gravity wave momentum flux in stratosphere and mesosphere. *Journal of Geophysical Research: Atmospheres*.

Gao, H., Li, L., Bu, L., Zhang, Q., Tang, Y., & Wang, Z. (2018). Effect of Small-Scale Gravity Waves on Polar Mesospheric Clouds Observed From CIPS/AIM. *Journal of Geophysical Research: Space Physics, 123(5),* 4026-4045.

669 Gerrard, A. J., Kane, T. J., Eckermann, S. D., & Thayer, J. P. (2004). Gravity waves and
670 mesospheric clouds in the summer middle atmosphere: A comparison of lidar measurements and
671 ray modeling of gravity waves over Sondrestrom, Greenland. *Journal of Geophysical Research:*
672 *Atmospheres, 109(D10)*.

673 Gumbel, J., & Karlsson, B. (2011). Intra-and inter-hemispheric coupling effects on the polar
674 summer mesosphere. *Geophysical research letters, 38(14)*.

675 Hervig, M. E., Gordley, L. L., Stevens, M. H., Russell III, J. M., Bailey, S. M., & Baumgarten,
676 G. (2009). Interpretation of SOFIE PMC measurements: Cloud identification and derivation of
677 mass density, particle shape, and particle size. *Journal of Atmospheric and Solar-Terrestrial*
678 *Physics, 316-330*.

679 Jensen, E. J., & Thomas, G. E. (1994). Numerical simulations of the effects of gravity waves on
680 noctilucent clouds. *Journal of Geophysical Research: Atmospheres, 99(D2)*, 3421-3430.

681 Kalisch, S., Preusse, P., Ern, M., Eckermann, S. D., & Riese, M. (2014). Differences in gravity
682 wave drag between realistic oblique and assumed vertical propagation. *Journal of Geophysical*
683 *Research: Atmospheres, 10-081*.

684 Karlsson, B., & Becker, E. (2016). How does interhemispheric coupling contribute to cool down
685 the summer polar mesosphere? *Journal of Climate*, 29(24), 8807-8821.

686 Karlsson, B., & Shepherd, T. G. (2018). The improbable clouds at the edge of the atmosphere.
687 *Physics today*, 30-36.

688 Karlsson, B., Körnich, H., & Gumbel, J. (2007). Evidence for interhemispheric stratosphere-
689 mesosphere coupling derived from noctilucent cloud properties. *Geophysical Research Letters,*
690 *34(16)*.

691 Karlsson, B., Randall, C. E., Benze, S., Mills, M., Harvey, V. L., Bailey, S. M., & Russell III, J.
692 M. (2009). Intra-seasonal variability of polar mesospheric clouds due to inter-hemispheric
693 coupling. *Geophysical research letters, 36(20)*.

694 Körnich, H., & Becker, E. (2010). A simple model for the interhemispheric coupling of the
695 middle atmosphere circulation. *Advances in Space Research*, 661-668.

696 Liu, H. L., & Rodle, R. G. (2002). A study of a self-generated stratospheric sudden warming and
697 its mesospheric-lower thermospheric impacts using the coupled TIME-GCM/CCM3. *Journal of*
698 *Geophysical Research: Atmospheres, 107(D23)*, 4695.

699 Matsuno, T. (1971). A dynamical model of the stratospheric sudden warming. *Journal of the*
700 *Atmospheric Sciences 28(8)*, 1479-1494.

701 McClintock, W. E. (2008). The cloud imaging and particle size experiment on the Aeronomy of
702 Ice in the mesosphere mission: Instrument concept, design, calibration, and on-orbit
703 performance. *Journal of atmospheric and solar-terrestrial physics*, 71(3-4), 340-355.

704 Preusse, P., Schroeder, S., Hoffmann, L., Ern, M., Friedl-Vallon, F., Ungermann, J., . . . Riese,
705 M. (2009). New perspectives on gravity wave remote sensing by spaceborne infrared limb
706 imaging. *Atmospheric Measurement Techniques*, 299-311.

Rapp, M., Lübken, F. J., Müllemann, A., Thomas, G. E., & Jensen, E. J. (2002). Small-scale temperature variations in the vicinity of NLC: Experimental and model results. *Journal of Geophysical Research: Atmospheres, 107(D19),* AAC-11.

Russell, J. M., Mlynczak, M. G., Gordley, L. L., Tansock, J. J., & Esplin, R. W. (1999). Overview of the SABER experiment and preliminary calibration results. *Optical Spectroscopic Techniques and Instrumentation for Atmospheric and Space Research III* (pp. 277-289). International Society for Optics and Photonics.

Sato, K., Watanabe, S., Kawatani, Y., Tomikawa, Y., Miyazaki, K., & Takahashi, M. (2009). On the origins of mesospheric gravity waves. *Geophysical research letters*.

Siskind, D. E., Eckermann, S. D., McCormack, J. P., Coy, L., Hoppel, K. W., & Baker, N. L. (2010). Case studies of the mesospheric response to recent minor, major, and extended stratospheric warmings. *Journal of Geophysical Research: Atmospheres, 115(D3)*.

Siskind, D. E., Stevens, M. H., Hervig, M., Sassi, F., Hoppel, K., Englert, C. R., & Kochenash, A. J. (2011). Consequences of recent southern hemisphere winter variability on polar mesospheric clouds. *Journal of atmospheric and solar-terrestrial physics*, 73(13) 2013-2021.

Thurairajah, B., Cullens, C. Y., Siskind, D. E., Hervig, M. E., & Bailey, S. M. (2020). The Role of Vertically and Obliquely Propagating Gravity Waves in Influencing the Polar Summer Mesosphere. *Journal of Geophysical Research: Atmospheres*, 125(9).

Thurairajah, B., Siskind, D. E., Bailey, S. M., Carstens, J. N., Russell III, J. M., & Mlynczak, M. G. (2017). Oblique propagation of monsoon gravity waves during the northern hemisphere 2007 summer. *Journal of Geophysical Research: Atmospheres*, 5063-5075.

Wright, C. J., & Gille, J. C. (2011). HIRDLS observations of gravity wave momentum fluxes over the monsoon regions. *Journal of Geophysical Research: Atmospheres*.

Yamashita, C., England, S. L., Immel, T. J., & Chang, L. C. (2013). Gravity wave variations during elevated stratopause events using SABER observations. *Journal of Geophysical Research: Atmospheres*, 5287-5303.

Yasui, R., Sato, K., & Tsutsumi, M. (2016). Seasonal and interannual variation of mesospheric gravity waves based on MF radar observations over 15 years at Syowa Station in the Antarctic. *SOLA, 12*, 46-50.